Electron Density and Compressibility in the Kitaev Model with a Spatially Modulated Phase in the Superconducting Pairing

condensed matter

MDPI

Article

Electron Density and Compressibility in the Kitaev Model with a Spatially Modulated Phase in the Superconducting Pairing

Fabián G. Medina Cuy and Fabrizio Dolcini *

Dipartimento di Scienza Applicata e Tecnologia, Politecnico di Torino, Corso Duca degli Abruzzi 24, 10129 Torino, Italy; fabian.medina@polito.it

* Correspondence: fabrizio.dolcini@polito.it

Abstract: A current flowing through a one-dimensional Kitaev chain induces a spatial modulation in its superconducting pairing, characterized by a wavevector Q, which is known to induce two types of topological phase transitions: one is the customary band topology transition between gapped phases, while the other is a Lifshitz transition related to the Fermi surface topology and leading to a gapless superconducting phase. We investigate the behavior of the electron density ρ and the compressibility κ across the two types of transitions, as a function of the model parameters. We find that the behavior of ρ as a function of Q and chemical potential μ enables one to infer the ground state phase diagram. Moreover, the analysis of the compressibility κ as a function of μ enables one to distinguish the two transitions: While κ exhibits a symmetric divergence across the band topology transition, it displays an asymmetric jump across the Lifshitz transition.

Keywords: Kitaev model; topological superconductors; p-wave superconductivity; topological transitions; Lifshitz transitions

1. Introduction

Topological superconductors (TSs) are considered to be extremely promising materials for frontier research in quantum science and technology. On the one hand, they exhibit Majorana zero modes (MZMs), exotic quasiparticles with nonlocal correlations and braiding properties that are suitable for fault-tolerant quantum computation. On the other hand, TSs are also characterized by dissipationless transport, which is an ideal feature for the development of energetically sustainable nanoelectronics [1–6]. Various platforms have been proposed for the experimental realization of 1D TSs, including proximized spin–orbit nanowires [7,8], quantum spin Hall edges [9,10] and ferromagnetic atom chains [11–15]. On the theory side, the essential properties of a p-wave TS are considered to be well captured by the Kitaev chain model, which exhibits two topologically distinct gapped phases, with MZMs appearing at the chain edges when the system is in the topologically non-trivial phase. Edge correlations therefore represent fingerprints of the topological phase transitions [16–19]. Generalizations of the Kitaev chain model including long-range hopping and superconducting terms have also been investigated, and can lead to algebraic decays of the correlation function in gapped phases [20–23].

Experiments on superconductor/semiconductor nanowires have focused on the search for zero-bias conductance peaks as the smoking gun evidence of MZMs, requiring an electrical current flow through the system. This has prompted researchers to investigate the effects of a spatially modulated phase in the superconducting pairing, where the modulation wavevector Q is proportional to the net momentum carried by a Cooper pair,

check for updates

Academic Editor: Yoram Dagan

Received: 31 January 2025
Revised: 21 February 2025
Accepted: 27 February 2025
Published: 28 February 2025

Citation: Medina Cuy, F.G.; Dolcini, F. Electron Density and Compressibility in the Kitaev Model with a Spatially Modulated Phase in the Superconducting Pairing. *Condens. Matter* **2025**, *10*, 14. https://doi.org/10.3390/condmat10010014

which is non-vanishing in the presence of a current flow [24–27]. Notably, a recent work showed that in the physically realistic regime where the superconducting pairing strength Δ_0 is smaller than the bandwidth energy parameter w ($\Delta_0 < w$), the phase modulation induces two types of phase transitions in the system: the first one is a transition in the band topology of the model, while the second one is a Lifshitz transition [28,29] from a gapped to a gapless superconducting phase [30,31]. Moreover, by treating Q as the wavevector of a synthetic dimension, a mapping has been established between the current carrying state of the 1D Kitaev model and the ground state of a 2D Weyl semimetal, where the gapless superconducting phase of the former corresponds to a type-II Weyl semimetal in the latter [32]. Another study analyzed the long-distance behavior of the correlation functions, showing that the system exhibits different types of exponential decays in the gapped phases and finding the period of the oscillatory algebraic decay in the gapless phases [33]. Furthermore, a connection was established between the gapless superconducting phase of the Kitaev chain and the chiral phase of spin models with Dzyaloshinskii–Moriya interaction [33].

Motivated by such promising results, in this work, we focus on two experimentally accessible quantities, namely the electron density and the compressibility, and analyze their behavior across the two types of topological transitions. This article is organized as follows: Section 2 describes the model and briefly summarizes the known properties of the ground state phase diagram as a function of Q and the chemical potential, recalling the parameter ranges for the gapped and gapless phases of the model. In Section 3, we present our results about the behavior of the density and compressibility across the boundaries of the two topological phase transitions. Section 4 is devoted to the discussion of the results and to our conclusions.

2. Materials and Methods

In this section, we briefly describe the model and summarize the main methodological aspects that are needed to investigate the behavior of the density and compressibility. More technical details can be found in Refs. [32,33].

2.1. Model and Ground State

The Kitaev chain model with a phase modulation of the superconducting p-wave pairing is described by the following second-quantized Hamiltonian:

$$\mathcal{H} = \sum_j \left[w\left(c_j^\dagger c_{j+1} + c_{j+1}^\dagger c_j\right) - \mu\left(c_j^\dagger c_j - \frac{1}{2}\right) + \Delta_0\left(e^{-iQ(2j+1)} c_j^\dagger c_{j+1}^\dagger + e^{iQ(2j+1)} c_{j+1} c_j\right)\right], \quad (1)$$

where $c_j^\dagger$ and c_j are electron creation and annihilation operators at the lattice site j. Here, $w > 0$ is the inter-site hopping energy, μ the chemical potential and $\Delta_0 > 0$ the strength of the superconducting pairing, while Q is the wavevector characterizing its spatial modulation and describing a current flow along the chain. We assume to deal with an infinitely long chain, where the number of sites is $N_s \gg 1$. By Fourier transform, we can rewrite the Hamiltonian (1) as

$$\mathcal{H} = \frac{1}{2} \sum_k \Psi_{k;Q}^\dagger H(k,Q) \Psi_{k;Q}, \quad (2)$$

where $\Psi_{k;Q}^\dagger = (c_{k-Q}^\dagger\,,\, c_{-k-Q})$ is the Nambu spinor, while the 2×2 matrix

$$H(k,Q) = h_0(k,Q)\sigma_0 + \vec{h}(k,Q) \cdot \vec{\sigma} \quad (3)$$

is the Bogoliubov–de Gennes Hamiltonian, where σ_0 is the identity matrix, $\vec{\sigma}$ is the vector $(\sigma_1, \sigma_2, \sigma_3)$ of Pauli matrices and

$$h_0(k,Q) = 2w\sin(Q)\sin(k), \tag{4}$$

$$\vec{h}(k,Q) = (0\,,\ \mathrm{Im}\{\Delta(k)\}\,,\ \xi(k,Q)) \tag{5}$$

with

$$\Delta(k) = 2\Delta_0 i\sin(k) \tag{6}$$

$$\xi(k,Q) = 2w\cos(Q)\cos(k) - \mu. \tag{7}$$

The single particle spectrum consists of an upper band E_+ and a lower band E_-, given by

$$E_\pm(k,Q) = h_0(k,Q) \pm \sqrt{\xi^2(k,Q) + |\Delta(k)|^2}. \tag{8}$$

Here, $\Delta(k)$ is odd under $k \to -k$, as clearly shown by Equation (6), and has a p-wave character. Thus, differently from s-wave superconductors, Δ_0 cannot be identified with the minimal spectral gap, which in general depends on Δ_0, μ and Q. This can be illustrated in the simple case of the customary Kitaev model ($Q = 0$). A few algebra steps show that, in the regime $\Delta_0 > w$, the minimal gap Δ_g of the spectrum (8) occurs at $k = 0$ for $\mu > 0$ or at $k = \pm\pi$ for $\mu < 0$, and is given by $\Delta_g = 2|2w - |\mu||$, regardless of the specific value of Δ_0. In contrast, in the regime $\Delta_0 < w$, the minimal gap occurs at a $\pm k^*$ (with $0 < |k^*| < \pi$) and depends also on the specific value of Δ_0. In particular, for $\mu = 0$, one has $\Delta_g = 4\Delta_0$.

As discussed in Refs. [32,33], for fixed values of Δ_0 and μ, depending on the value of the spatial modulation Q, the spectrum (8) can be either gapped, or characterized by a direct gap closing occurring at $k = 0, \pi$, or even exhibit an indirect gap closing, if Q is sufficiently large. In the latter case, the occupancy of the bands changes, modifying the physical nature of the ground state from a gapped to a gapless superconductor. Thus, the ground state is in general characterized by three sectors of the Brillouin zone: the Cooper pair sector S_p, the unpaired electron sector S_e and the unpaired hole sector S_h. These three sectors form the entire Brillouin zone as $\mathrm{BZ} \equiv S_p \cup S_e \cup S_h$. We will also refer to the unpaired sector as the region $S_u = S_e \cup S_h$. The ground state takes the general expression

$$|G(Q)\rangle = \prod_{\substack{0<k<\pi \\ k\in S_p}} \left(u_Q(k) + v_Q^*(k) c_{-k-Q}^\dagger c_{k-Q}^\dagger\right) \prod_{k\in S_e} c_{k-Q}^\dagger\,|0\rangle\,, \tag{9}$$

where

$$u_Q(k) = \sqrt{\frac{1}{2}\left(1 + \frac{\xi(k,Q)}{h(k,Q)}\right)}, \quad v_Q(k) = -i\mathrm{sgn}(\sin(k))\sqrt{\frac{1}{2}\left(1 - \frac{\xi(k,Q)}{h(k,Q)}\right)} \tag{10}$$

are the weights of the eigenstates $(u_Q(k),\ v_Q(k))^T$ and $(-v_Q^*(k),\ u_Q(k))^T$ of Equation (3).

Before concluding this subsection, we would like to highlight a few differences between our model Equation (1) and the model for an FFLO state [34,35]. Although in both cases, the superconducting pairing is characterized by a spatial modulation, in the FFLO case, its wavevector Q is related to an exchange field, typically due to ferromagnetic impurities and acting on the electron spin, whereas here we are considering a spinless model, and Q originates from a current flow. Moreover, the FFLO is an equilibrium state, whereas Equation (9) describes a current-carrying (stationary) out-of-equilibrium state. As a consequence, the spatially modulated pairing is real in the FFLO case [36–38], while in Equation (1), it exhibits a complex phase, yielding a current.

2.2. Gapped and Gapless Phases in the Kitaev Model

One can identify two distinct regimes, depending on the value of the pairing strength Δ_0. For $\Delta_0 > w$, only gapped phases essentially exist. This is illustrated in Figure 1a, where the trivial (topological) gapped phase is denoted in gray (pink) color, as a function of Q and μ. The two gapped phases are separated by two separatrix curves (black lines), along which the spectral gap closes *directly*. In contrast, for $\Delta_0 < w$, the spectral gap closes *indirectly* and the gapless phase emerges in the Q-μ phase diagram, as highlighted in green in Figure 1b.

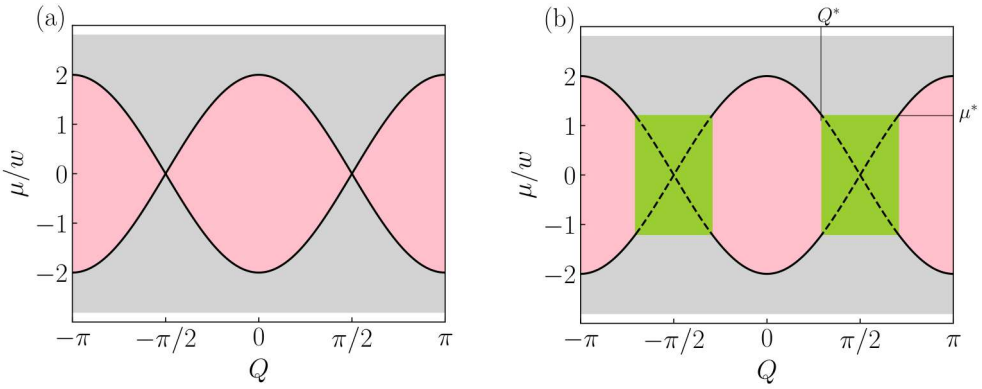

Figure 1. Phase diagram of the Kitaev chain as a function of the superconducting phase wavevector Q and the chemical potential μ, for two regimes of the system (**a**) $\Delta_0 = 1.4w$ and (**b**) $\Delta_0 = 0.8w$. The pink and gray regions correspond to the topological and trivial gapped phases, respectively, while the green regions identify the gapless phases. The values Q^* and μ^* characterizing the boundaries of the gapless phases are given in Equations (18) and (19).

2.2.1. Gapped Phases

Gapped phases are identified by the condition that $E_+(k, Q) > 0$ and $E_-(k, Q) < 0$ for all $k \in$ BZ. In this case, it can be shown [33] that the paired sector covers the entire Brillouin zone, while the unpaired sectors are empty:

$$\begin{aligned} S_p &\equiv \text{BZ} \leftrightarrow k \in [-\pi, \pi] \\ S_e &= S_h = \varnothing \end{aligned} \quad . \tag{11}$$

Then, the general expression (9) of the ground state reduces to the standard form consisting of Cooper pairs only. The system is in a gapped phase if one of the three following conditions is met:

$$\begin{aligned} &(1) \quad |\mu| > 2w \quad \text{and} \quad \forall \Delta_0 > 0 \text{ and } \forall Q; \\ &(2) \quad |\mu| < 2w \quad \text{and} \quad \sqrt{w^2 - \mu^2/4} < \Delta_0 \text{ and } |\cos(Q)| \neq |\mu|/2w; \\ &(3) \quad |\mu| < 2w \quad \text{and} \quad w|\sin(Q)| < \Delta_0 < \sqrt{w^2 - \mu^2/4}. \end{aligned} \tag{12}$$

As one can notice from the phase diagram in Figure 1, the condition (1) in Equation (12) corresponds to a trivial phase of the system, and conditions (2) and (3) can be either topological or trivial. Note that the second condition in (12) excludes the separatrix curves, given by

$$\mu_c^{\pm}(Q) = \pm 2w \cos Q \tag{13}$$

identified by the solid and dashed black lines of the phase diagrams in Figure 1.

2.2.2. Gapless Phases

Gapless phases emerge when $E_\pm(k,Q) < 0$ or $E_\pm(k,Q) > 0$ for some values of k. The conditions for the system to be in a gapless phase are [32,33]

$$\sqrt{w^2 - \mu^2/4} > \Delta_0 \quad \text{and} \quad w|\sin(Q)| > \Delta_0. \tag{14}$$

In this case, the sectors in k space for paired and unpaired fermions are

$$S_p = \{k \,|\, 0 < |k| < |k^*_-| \quad \text{and} \quad \pi - |k^*_+| < |k| < \pi\}, \tag{15}$$

and

$$S_u = \{k \,|\, |k^*_-| < |k| < \pi - |k^*_+|\}, \tag{16}$$

where

$$k^*_\pm = \arcsin\left(\frac{\cos(Q)}{\sqrt{1-\frac{\Delta_0^2}{w^2}}}\right) \pm \arcsin\left(\frac{\mu}{2w\sqrt{1-\frac{\Delta_0^2}{w^2}}}\right). \tag{17}$$

The condition (14) determines the values of Q^* and μ^* at which the system is at the boundary between the gapped and gapless phase, as highlighted in Figure 1b. These values are given by

$$Q^* = \arcsin\left(\frac{\Delta_0}{w}\right) \tag{18}$$

and

$$\mu^* = 2\sqrt{w^2 - \Delta_0^2}. \tag{19}$$

Note that the system is in the gapless phases if $Q^* < |Q| < \pi - Q^*$ and $|\mu| < \mu^*$.

3. Results

Here, we present our results about the electron density

$$\rho = \langle c_j^\dagger c_j \rangle, \tag{20}$$

where $\langle \cdots \rangle$ denotes the expectation value taken with respect to the ground state (9). In order to explicitly evaluate ρ, one can re-express $c_j = N_s^{-1/2} \sum_{k \in BZ} e^{ikj} c_k$ in terms of its Fourier modes c_k's, and exploit the correlation functions in k space, where the Brillouin zone sectors S_p, S_e and S_h contribute differently [33]. In particular, it turns out that only the sector S_p of Cooper pairs contributes to the density. After taking the thermodynamic limit, ρ can be therefore re-expressed as

$$\rho = \frac{1}{2} + \Delta\rho, \tag{21}$$

where

$$\Delta\rho = -\frac{1}{4\pi} \int_{S_p} dk \frac{\xi(k,Q)}{\sqrt{\xi^2(k,Q) + |\Delta(k)|^2}} \tag{22}$$

describes the deviation from the half filling density value $1/2$. We recall that, if the system is in a gapped phase, the S_p sector coincides with the entire Brillouin zone (see Equation (11)), while in the gapless phase, S_p is strictly smaller than the Brillouin zone and is controlled by the chemical potential μ and the modulation wavevector Q (see (15)).

Figure 2 shows $\Delta\rho$ as a function of the modulation wavevector Q and the chemical potential μ. The two panels (a) and (b) refer to the same two values $\Delta_0 = 1.4w$ and $\Delta_0 = 0.8w$ used in the two panels of Figure 1, respectively. The first feature one can

notice from Figure 2 is that, for $\mu = 0$, one has $\Delta\rho = 0$, regardless of the value of the spatial modulation Q and the superconducting pairing strength Δ_0. This means that $\mu = 0$ always corresponds to the half filling density value $\rho = 1/2$. This property can be shown with a little algebra from Equation (22), and originates from the chiral symmetry of the Hamiltonian (1), which at $\mu = 0$ is invariant under the (anti-unitary) transformation $\mathcal{S} c_j \mathcal{S}^{-1} = (-1)^j c_j^\dagger$ [33]. The second noteworthy aspect in the behavior of the electron density shown in Figure 2 is that it straightforwardly reflects the ground state phase diagrams shown in Figure 1. In particular, in Figure 2a, the density behavior enables one to clearly distinguish the separatrix Equation (13) between the two gapped phases (black curves of Figure 1a), while Figure 2b allows one to identify the wavevector Q^* and the chemical potential value μ^* (see Equations (18) and (19)) characterizing the onset of the gapless phases shown in Figure 1b.

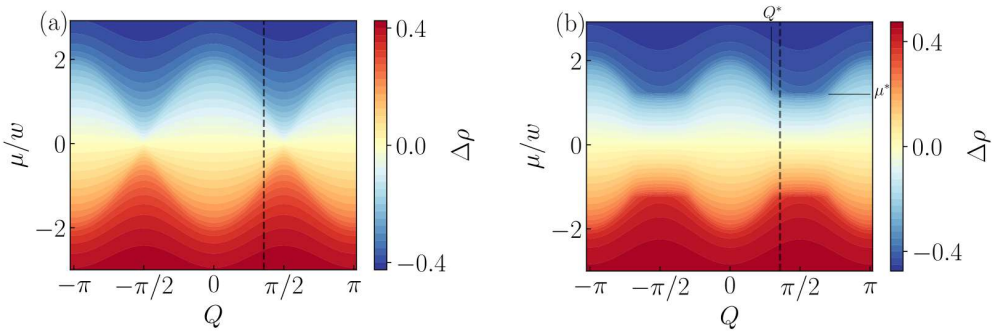

Figure 2. Contour plot of the density deviation $\Delta\rho$ as a function of Q and μ. (**a**) Regime of only gapped phases with $\Delta_0 = 1.4w$. (**b**) Regime where gapless phases emerge for some values of Q and μ, with $\Delta_0 = 0.8w$. The values of Q^* and μ^* signal the location of the gapless boundaries and are given by (18) and (19), respectively. The vertical dashed line corresponds to a cut at $Q = \pi/3$ (see Figure 3).

In order to gain further information from the behavior of the density $\Delta\rho$, we have analyzed its μ-dependence at a fixed value $Q = \pi/3$ of the modulation wavevector, highlighted by a black vertical dashed line in both panels of Figure 2. We start by examining the case $\Delta_0 > w$. Figure 3a represents the cut of Figure 2a at $Q = \pi/3$ as a function of μ, in the range $0 < \mu < 3w$, and the vertical green dashed line highlights the value of $\mu_c = \mu_c^+(\pi/3)$ (see Equation (13)), corresponding to the separatrix between the trivial and the topological gapped phases. A close inspection of the curve shows that it exhibits a kink at the critical value μ_c. However, such a singular behavior can be better revealed by analyzing the compressibility

$$\kappa = \frac{1}{\rho^2} \frac{\partial \rho}{\partial \mu} \quad , \tag{23}$$

which is shown in Figure 3b. A divergence at μ_c is clearly visible in κ, from both the topological and the trivial side of the transition, indicated by the black and red dashed curves in Figure 3b, respectively. By analyzing such a divergence, we have found a power-law behavior $\kappa \sim 1/|\mu - \mu_c|^b$ for $\mu \to \mu_c$, characterized by the same exponent b from both sides of the transition. This is clearly shown in the log–log plot of Figure 3c, which illustrates $\ln|\kappa|$, as a function of $\ln|\mu - \mu_c|$. Here, black dots represent values for $\mu < \mu_c$ and red dots for $\mu > \mu_c$, and they both overlap onto the same dashed–dotted blue line, which represents a linear fit of the ten points closest to μ_c, returning a value $b \simeq 0.13$ for the exponent, for the above model parameters. This symmetrical divergence from both the topological and the trivial side is consistent with previous studies on correlation functions in topological systems [39], and highlights the fact that, differently from the conventional Landau phase transition scheme, two topologically distinct phases are not straightforwardly identified by the onset of an order parameter.

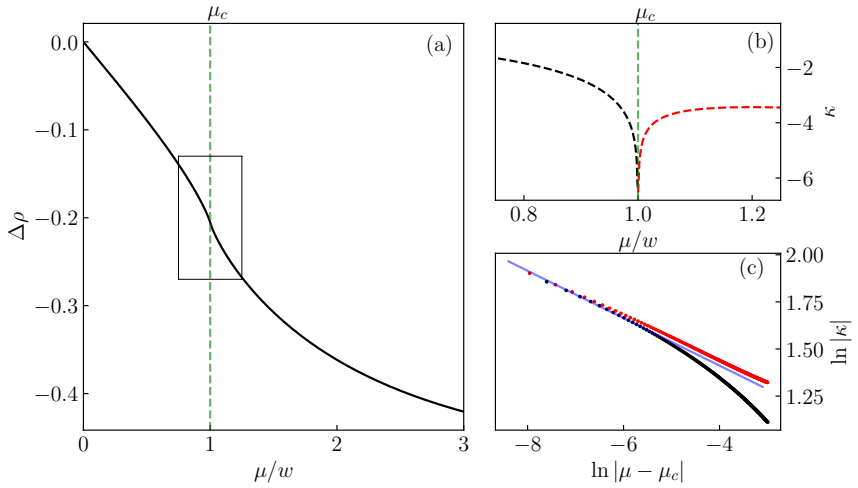

Figure 3. Cut of Figure 2a at $Q = \pi/3$. (**a**) The density deviation $\Delta\rho$ is shown as a function of μ. (**b**) The compressibility (23) is plotted as a function of μ in the range within the black rectangle in panel (**a**). (**c**) The log–log plot of the compressibility shows a symmetric power-law singularity behavior for the compressibility $\kappa \sim |\mu - \mu_c|^b$, where black and red data correspond to the ranges $\mu < \mu_c$ (topological gapped phase) and $\mu > \mu_c$ (trivial gapped phase), respectively. The ten closer points to Q_c were fitted with $\ln|\kappa| = a - b\ln|\mu - \mu_c|$, where $a \sim 0.91$ and $b \sim 0.13$.

Let us now turn to the regime $\Delta_0 < w$, and analyze the gapped–gapless superconductor transition. Figure 4a shows the Q-cut of the contour plot in Figure 2b at $Q = \pi/3$. Here, the vertical green dashed line highlights the boundary μ^* between the trivial gapped phase and the gapless phase, given by Equation (19) and shown also in Figure 2b. As one can see, the kink in the curve Figure 4a is now more pronounced than the one in Figure 3a. The reason is revealed by the analysis of the compressibility (23) displayed in Figure 4b: in striking contrast to the case of the transition across two gapped phases, the compressibility across the gapped-to-gapless transition exhibits an *asymmetric jump* at μ^*. Specifically, while from the gapped side of the transition ($\mu > \mu^*$), κ is *finite*, from the gapless side of the transition ($\mu < \mu^*$), it diverges. This effect is similar to the one predicted in Ref. [33] for the anomalous correlator, as a function of Q though.

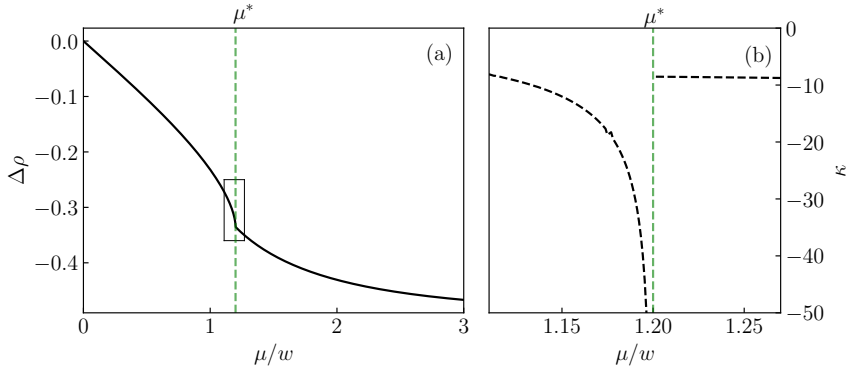

Figure 4. Cut of Figure 2b at $Q = \pi/3$. (**a**) The density deviation $\Delta\rho$ is shown as a function of μ. The vertical green dashed line corresponds to the value μ^* given by (19), which is the boundary between gapped and gapless phases. (**b**) The compressibility (23) is plotted as a function of μ in the range within the black rectangle in panel (**a**). An asymmetric jump can be seen at μ^*; namely, from the gapped side of the transition ($\mu > \mu_c$), κ tends to a finite value, while it diverges from the gapless side ($\mu < \mu_c$).

Case $Q = \pm\pi/2$

We have already observed above that for $\mu = 0$, the integral in Equation (22) vanishes, reflecting the chiral symmetry acquired by the Hamiltonian, and yielding the half filling value $\rho = 1/2$ for the density, at any value of Q and Δ_0. There exists another special parameter value, at which an analytical expression for $\Delta\rho$ can be found, namely $Q = \pm\pi/2$. Indeed, in this case, model (1) exhibits another symmetry; i.e., it is invariant under the (unitary) spatial inversion $\mathcal{I} c_j \mathcal{I}^{-1} = c_{-j}$ [33]. This enables one to rewrite Equation (22) as

$$\Delta\rho = \frac{\mathrm{sgn}(\mu)}{\pi} F\left(\alpha; -4\delta_\mu\right), \tag{24}$$

where $F(\alpha; -4\delta_\mu)$ is the elliptic integral of the first kind. Here, $\delta_\mu = \Delta_0^2/\mu^2$, while α takes different values depending on the phase. Specifically, for the gapped phase, $\alpha = \pi/2$, while for the gapless phase, one has

$$\alpha = \arcsin\left(\frac{|\mu|}{2\sqrt{w^2 - \Delta_0^2}}\right). \tag{25}$$

4. Discussion and Conclusions

We have investigated the 1D Kitaev chain model in the presence of a phase modulation of the superconducting pairing, which describes a current flowing through the chain. Such modulation is known to induce two types of effects. On the one hand, it affects the customary band topology transition by modifying the separatrix between the topological and trivial gapped phases, where the spectral gap closes directly. On the other hand, in the physically realistic parameter regime $\Delta_0 < w$, it can lead to a Lifshitz transition, i.e., a topological change in the Fermi surface. This corresponds to the appearance of a gapless superconductor phase (see Figure 1), characterized by an indirect spectral gap closing.

Here, we have analyzed the behavior of the electron density ρ and the compressibility κ across these two types of topological transitions. We have found that the behavior of the density as a function of the phase modulation wavevector Q and the chemical potential μ (Figure 2) is quite informative to infer the phase diagram of Figure 1. In particular, in the regime $\Delta_0 > w$, it enables one to identify the separatrix (13) between the gapped phases (Figure 1a), while in the regime $\Delta_0 < w$, one can extract the boundary values Q^* and μ^* (see Equations (18) and (19)) characterizing the gapless phase. Moreover, the analysis of the compressibility (23) enables one to operatively distinguish between the two types of transitions. Indeed, the customary band topology transition between topologically different gapped phases is characterized by a *symmetric* power-law divergence of κ at the critical value μ_c (see Figure 3b), with the same exponent both from the trivial and the topological side of the transition. In contrast, across the gapped–gapless transition, κ is characterized by an *asymmetric jump* at μ^*: while it tends to a finite value from the gapped side, it diverges from the gapless side of the transition (see Figure 4b).

We conclude by outlining possible experimental setups, where our results could be tested. Two types of platforms seem promising for the realization of 1D topological superconductors. The first one is based on InSb and InAs nanowires proximized by a superconducting film (e.g., Al or Nb) and exposed to a magnetic field [40–45], while the second one consists of ferromagnetic atom chains deposited on a superconducting film [46–48]. Electron density profile in semiconductors can be locally probed with various techniques such as atomic force microscopy, capacitance voltage measurements and X-ray reflectivity [49–53]. The chemical potential can be controlled by a gate voltage, and the compressibility of electron gases in semiconductors can be measured with capac-

itive techniques [54]. Moreover, scanning tunneling microscopy has been proposed as a technique to measure local correlation functions in magnetic atom chains [11,12].

Author Contributions: Conceptualization, F.G.M.C. and F.D.; methodology, F.G.M.C. and F.D.; software, F.G.M.C.; validation, F.G.M.C. and F.D.; formal analysis, F.G.M.C. and F.D.; investigation, F.G.M.C. and F.D.; resources, F.G.M.C. and F.D.; data curation, F.G.M.C.; writing—original draft preparation, F.G.M.C. and F.D.; writing—review and editing, F.G.M.C. and F.D.; visualization, F.G.M.C.; supervision, F.D.; project administration, F.D.; funding acquisition, F.D. All authors have read and agreed to the published version of the manuscript.

Funding: F.G.M.C. acknowledges financial support from ICSC Centro Nazionale di Ricerca in High-Performance Computing, Big Data, and Quantum Computing (Spoke 7), Grant No. CN00000013, funded by European Union NextGeneration EU. F.D. acknowledges the financial support from the TOPMASQ project, CUP E13C24001560001, funded by the National Quantum Science and Technology Institute (Spoke 5), Grant No. PE0000023, funded by the European Union—NextGeneration EU.

Institutional Review Board Statement: Not applicable.

Informed Consent Statement: Not applicable.

Data Availability Statement: All the data in this study are available within this paper.

Acknowledgments: We thanks Lorenzo Rossi for fruitful discussions.

Conflicts of Interest: The funders had no role in the design of the study; in the collection, analyses, or interpretation of data; in the writing of the manuscript; or in the decision to publish the results.

References

1. Kitaev, A.Y. Fault-tolerant quantum computation by anyons. *Ann. Phys.* **2003**, *303*, 2–30. [CrossRef]
2. Alicea, J. New directions in the pursuit of Majorana fermions in solid state systems. *Rep. Prog. Phys.* **2012**, *75*, 076501. [CrossRef] [PubMed]
3. Aguado, R. Majorana quasiparticles in condensed matter. *Riv. Nuovo Cimento* **2017**, *40*, 523–593. [CrossRef]
4. Lian, B.; Sun, X.Q.; Vaezi, A.; Qi, X.L.; Zhang, S.C. Topological quantum computation based on chiral Majorana fermions. *Proc. Natl. Acad. Sci. USA* **2018**, *115*, 10938–10942. [CrossRef] [PubMed]
5. Das Sarma, S. In search of Majorana. *Nat. Phys.* **2023**, *19*, 165–170. [CrossRef]
6. Aghaee, M.; Akkala, A.; Alam, Z.; Ali, R.; Ramirez, A.A.; Andrzejczuk, M.; Antipov, A.E.; Aseev, P.; Astafev, M.; Bauer, B.; et al. InAs-Al hybrid devices passing the topological gap protocol. *Phys. Rev. B* **2023**, *107*, 245423. [CrossRef]
7. Lutchyn, R.M.; Sau, J.D.; Das Sarma, S. Majorana fermions and a topological phase transition in semiconductor-superconductor heterostructures. *Phys. Rev. Lett.* **2010**, *105*, 077001. [CrossRef] [PubMed]
8. Oreg, Y.; Refael, G.; von Oppen, F. Helical Liquids and Majorana Bound States in Quantum Wires. *Phys. Rev. Lett.* **2010**, *105*, 177002. [CrossRef] [PubMed]
9. Fu, L.; Kane, C.L. Superconducting proximity effect and Majorana fermions at the surface of a topological insulator. *Phys. Rev. Lett.* **2008**, *100*, 096407. [CrossRef] [PubMed]
10. Fu, L.; Kane, C.L. Josephson current and noise at a superconductor/quantum-spin-Hall-insulator/superconductor junction. *Phys. Rev. B* **2009**, *79*, 161408. [CrossRef]
11. Choy, T.P.; Edge, J.M.; Akhmerov, A.R.; Beenakker, C.W.J. Majorana fermions emerging from magnetic nanoparticles on a superconductor without spin-orbit coupling. *Phys. Rev. B* **2011**, *84*, 195442. [CrossRef]
12. Nadj-Perge, S.; Drozdov, I.K.; Bernevig, B.A.; Yazdani, A. Proposal for realizing Majorana fermions in chains of magnetic atoms on a superconductor. *Phys. Rev. B* **2013**, *88*, 020407. [CrossRef]
13. Pientka, F.; Glazman, L.I.; von Oppen, F. Topological superconducting phase in helical Shiba chains. *Phys. Rev. B* **2013**, *88*, 155420. [CrossRef]
14. Vazifeh, M.M.; Franz, M. Self-Organized Topological State with Majorana Fermions. *Phys. Rev. Lett.* **2013**, *111*, 206802. [CrossRef]
15. Heimes, A.; Kotetes, P.; Schön, G. Majorana fermions from Shiba states in an antiferromagnetic chain on top of a superconductor. *Phys. Rev. B* **2014**, *90*, 060507. [CrossRef]
16. Miao, J.J.; Jin, H.K.; Zhang, F.C.; Zhou, Y. Exact Solution for the Interacting Kitaev Chain at the Symmetric Point. *Phys. Rev. Lett.* **2017**, *118*, 267701. [CrossRef] [PubMed]

17. Wang, Y.; Miao, J.J.; Jin, H.K.; Chen, S. Characterization of topological phases of dimerized Kitaev chain via edge correlation functions. *Phys. Rev. B* **2017**, *96*, 205428. [CrossRef]
18. Miao, J.J.; Jin, H.K.; Zhang, F.C.; Zhou, Y. Majorana zero modes and long range edge correlation in interacting Kitaev chains: Analytic solutions and density-matrix-renormalization-group study. *Sci. Rep.* **2018**, *8*, 488. [CrossRef]
19. Koga, A.; Murakami, Y.; Nasu, J. Majorana correlations in the Kitaev model with ordered-flux structures. *Phys. Rev. B* **2021**, *103*, 214421. [CrossRef]
20. Vodola, D.; Lepori, L.; Ercolessi, E.; Gorshkov, A.V.; Pupillo, G. Kitaev Chains with Long-Range Pairing. *Phys. Rev. Lett.* **2014**, *113*, 156402. [CrossRef]
21. Vodola, D.; Lepori, L.; Ercolessi, E.; Pupillo, G. Long-range Ising and Kitaev models: Phases, correlations and edge modes. *New J. Phys.* **2016**, *18*, 015001. [CrossRef]
22. Jäger, S.B.; Dell'Anna, L.; Morigi, G. Edge states of the long-range Kitaev chain: An analytical study. *Phys. Rev. B* **2020**, *102*, 035152. [CrossRef]
23. Francica, G.; Dell'Anna, L. Correlations, long-range entanglement, and dynamics in long-range Kitaev chains. *Phys. Rev. B* **2022**, *106*, 155126. [CrossRef]
24. Takasan, K.; Sumita, S.; Yanase, Y. Supercurrent-induced topological phase transitions. *Phys. Rev. B* **2022**, *106*, 014508. [CrossRef]
25. Kotetes, P. Diagnosing topological phase transitions in 1D superconductors using Berry singularity markers. *J. Phys. Cond. Mater.* **2022**, *34*, 174003. [CrossRef]
26. Ma, E.S.; Song, Z. Off-diagonal long-range order in the ground state of the Kitaev chain. *Phys. Rev. B* **2023**, *107*, 205117. [CrossRef]
27. Maiellaro, A.; Romeo, F.; Illuminati, F.; Citro, R. Resilience of topological superconductivity under particle current. *Phys. Rev. B* **2023**, *107*, 064505. [CrossRef]
28. Volovik, G. Topological lifshitz transitions. *Low Temp. Phys.* **2017**, *43*, 47–55. [CrossRef]
29. Volovik, G.E. Exotic Lifshitz transitions in topological materials. *Phys. Usp.* **2018**, *61*, 89. [CrossRef]
30. Yerin, Y.; Petrillo, C.; Varlamov, A. The Lifshitz nature of the transition between the gap and gapless states of a superconductor. *SciPost* **2022**, *5*, 009. [CrossRef]
31. Yerin, Y.; Varlamov, A.; Petrillo, C. Topological nature of the transition between the gap and the gapless superconducting states. *Europhys. Lett.* **2022**, *138*, 16005. [CrossRef]
32. Medina Cuy, F.G.; Buccheri, F.; Dolcini, F. Lifshitz transitions and Weyl semimetals from a topological superconductor with supercurrent flow. *Phys. Rev. Res.* **2024**, *6*, 033060. [CrossRef]
33. Medina Cuy, F.G.; Dolcini, F. Correlation functions of the Kitaev model with a spatially modulated phase in the superconducting order parameter. *Phys. Rev. B* **2024**, *110*, 214512. [CrossRef]
34. Fulde, P.; Ferrell, R.A. Superconductivity in a Strong Spin-Exchange Field. *Phys. Rev.* **1964**, *135*, A550–A563. [CrossRef]
35. Larkin, A.I.; Ovchinnikov, Y.N. Nonuniform state of Superconductors. *Zh. Eksp. Teor. Fiz.* **1964**, *47*, 1136–1146; English version in *Sov. Phys. J. Exp. Theor. Phys.* **1965**, *20*, 762.
36. Machida, K.; Nakanishi, H. Superconductivity under a ferromagnetic molecular field. *Phys. Rev. B* **1984**, *30*, 122–133. [CrossRef]
37. Buzdin, A.I.; Polonskiĭ, S.V. Nonuniform state in quasi-1D superconductors. *Sov. Phys. J. Exp. Theor. Phys.* **1987**, *66*, 422–429.
38. Matsuda, Y.; Shimahara, H. Fulde-Ferrell-Larkin-Ovchinnikov state in heavy fermion superconductors. *J. Phys. Soc. Jpn.* **2007**, *76*, 051005. [CrossRef]
39. Chen, W.; Legner, M.; Rüegg, A.; Sigrist, M. Correlation length, universality classes, and scaling laws associated with topological phase transitions. *Phys. Rev. B* **2017**, *95*, 075116. [CrossRef]
40. Mourik, V.; Zuo, K.; Frolov, S.; Plissard, S.; Bakkers, E.P.A.M.; Kouwenhoven, L. Signatures of Majorana fermions in hybrid superconductor-semiconductor nanowire devices. *Science* **2012**, *336*, 1003–1007. [CrossRef]
41. Rokhinson, L.P.; Liu, X.; Furdyna, J.K. The fractional ac Josephson effect in a semiconductor–superconductor nanowire as a signature of Majorana particles. *Nat. Phys.* **2012**, *8*, 795–799. [CrossRef]
42. Das, A.; Ronen, Y.; Most, Y.; Oreg, Y.; Heiblum, M.; Shtrikman, H. Zero-bias peaks and splitting in an Al–InAs nanowire topological superconductor as a signature of Majorana fermions. *Nat. Phys.* **2012**, *8*, 887–895. [CrossRef]
43. Gül, Ö.; Zhang, H.; Bommer, J.D.; de Moor, M.W.; Car, D.; Plissard, S.R.; Bakkers, E.P.; Geresdi, A.; Watanabe, K.; Taniguchi, T.; et al. Ballistic Majorana nanowire devices. *Nat. Nanotechnol.* **2018**, *13*, 192–197. [CrossRef] [PubMed]
44. Hart, S.; Ren, H.; Wagner, T.; Leubner, P.; Mühlbauer, M.; Brüne, C.; Buhmann, H.; Molenkamp, L.W.; Yacoby, A. Induced superconductivity in the quantum spin Hall edge. *Nat. Phys.* **2014**, *10*, 638–643. [CrossRef]
45. Yu, P.; Chen, J.; Gomanko, M.; Badawy, G.; Bakkers, E.; Zuo, K.; Mourik, V.; Frolov, S. Non-Majorana states yield nearly quantized conductance in proximatized nanowires. *Nat. Phys.* **2021**, *17*, 482–488. [CrossRef]
46. Nadj-Perge, S.; Drozdov, I.K.; Li, J.; Chen, H.; Jeon, S.; Seo, J.; MacDonald, A.H.; Bernevig, B.A.; Yazdani, A. Observation of Majorana fermions in ferromagnetic atomic chains on a superconductor. *Science* **2014**, *346*, 602–607. [CrossRef]
47. Chen, H.J.; Fang, X.W.; Chen, C.Z.; Li, Y.; Tang, X.D. Robust signatures detection of Majorana fermions in superconducting iron chains. *Sci. Rep.* **2016**, *6*, 36600. [CrossRef]

48. Pawlak, R.; Kisiel, M.; Klinovaja, J.; Meier, T.; Kawai, S.; Glatzel, T.; Loss, D.; Meyer, E. Probing atomic structure and Majorana wavefunctions in mono-atomic Fe chains on superconducting Pb surface. *Npj Quant. Inf.* **2016**, *2*, 16035. [CrossRef]
49. Suresh, N.; Phase, D.; Gupta, A.; Chaudhari, S. Electron density fluctuations at interfaces in Nb/Si bilayer, trilayer, and multilayer films: An x-ray reflectivity study. *J. Appl. Phys.* **2000**, *87*, 7946–7958. [CrossRef]
50. Garnett, E.C.; Tseng, Y.C.; Khanal, D.R.; Wu, J.; Bokor, J.; Yang, P. Dopant profiling and surface analysis of silicon nanowires using capacitance-voltage measurements. *Nat. Nanotechnol.* **2009**, *4*, 311–314. [CrossRef] [PubMed]
51. Rojo, M.M.; Calero, O.C.; Lopeandia, A.; Rodriguez-Viejo, J.; Martín-Gonzalez, M. Review on measurement techniques of transport properties of nanowires. *Nanoscale* **2013**, *5*, 11526–11544. [CrossRef] [PubMed]
52. Wielgoszewski, G.; Pałetko, P.; Tomaszewski, D.; Zaborowski, M.; Jóźwiak, G.; Kopiec, D.; Gotszalk, T.; Grabiec, P. Carrier density distribution in silicon nanowires investigated by scanning thermal microscopy and Kelvin probe force microscopy. *Micron* **2015**, *79*, 93–100. [CrossRef]
53. Kim, S.; Lee, H.; Eom, S.; Ji, G.; Choi, S.H.; Joo, H.; Bae, J.; Kim, K.K.; Park, H.R.; Park, K.D. Dynamical control of nanoscale electron density in atomically thin n-type semiconductors via nano-electric pulse generator. *Sci. Adv.* **2024**, *10*, eadr0492. [CrossRef]
54. Eisenstein, J.; Pfeiffer, L.; West, K. Compressibility of the two-dimensional electron gas: Measurements of the zero-field exchange energy and fractional quantum Hall gap. *Phys. Rev. B* **1994**, *50*, 1760–1778. [CrossRef]